RSC Advances

PAPER

View Article Online
View Journal | View Issue

Cite this: *RSC Adv.*, 2017, **7**, 7198

Optical thermometry based on thermal population of low-lying levels of Eu^{3+} in $Ca_{2.94}Eu_{0.04}Sc_2Si_3O_{12}$

Lu Zhao, Jiajia Cai, Fangfang Hu, Xinyue Li, Zhongmin Cao, Xiantao Wei, Yonghu Chen, Min Yin* and Chang-Kui Duan*

Non-contact optical thermometry using rare-earth materials has attracted a lot of attention due to its realization of non-invasive and real-time temperature determination. In the current work, a new mechanism, differing from the conventional approach utilizing the ratio of intensities emitted from two thermally coupled excited levels, was developed and demonstrated for temperature sensing using Eu^{3+}-doped $Ca_3Sc_2Si_3O_{12}$ (CSSO). Under the excitation of 610.6 nm-wavelength light, Eu^{3+} ions at the $^7F_2$ multiplet became excited to the $^5D_0$ state, and then the luminescence intensity originating from the $^5D_0$ state increased significantly as the temperature was increased from 123 K to 273 K. The thermoequilibrium of the $^7F_2$ multiplet with the $^7F_0$ ground state at a weak excitation ensured a steady increase of the luminescence intensity I with temperature T, which well fit the equation $I = A \exp(-B/T)$ for the transitions to both $^7F_1$ and $^7F_4$ multiplets. A relative sensitivity S_R of $1008/T^2$ was obtained for the $^7F_1$ case, with a value of 1.35% at 273 K. This scheme, as a result of detecting the blue-shifted emission, has the advantages of being less disturbed by stray light from the host and the object of the thermometry. In addition, the high quantum efficiency of a one-photon excited photoluminescence scheme has the advantage of improving the resolution of the thermometry. Furthermore, a near-infrared broadband emission observed in the sample can be adopted as a reference, so as to transform the scheme into one using a luminescence intensity ratio. These results indicated that CSSO:Eu^{3+} may be used in practical temperature sensing applications.

Received 20th December 2016
Accepted 9th January 2017

DOI: 10.1039/c6ra28431k

www.rsc.org/advances

1. Introduction

Temperature-dependent luminescence properties of materials based on rare earth elements have been widely studied for their applications in non-contact optical thermometry.[1–4] Many of these investigations have focused on the fluorescence intensity ratio (FIR) of two thermally coupled excited energy levels (TCEELs) of rare earth ions such as Pr^{3+},[5] Nd^{3+},[6,7] Gd^{3+},[8] Dy^{3+},[9,10] Ho^{3+},[11,12] Er^{3+},[13–18] and Tm^{3+},[19] and have frequently involved up-conversion (UC) luminescence.[6,8,11–16,19] In particular, the FIR technique based on TCEELs has the advantage of requiring few measurements since it is not susceptible to fluctuations of excitation power. However, these FIR schemes suffer from the loss of thermal coupling at low temperatures, causing a deviation of the luminescence intensity ratio from that predicted by the Boltzmann distribution law. As a result, the energy difference between the two levels is usually restrained to be in the range of 200–2000 cm^{-1}.[20] The mechanism for the transitions involved in the FIR method based on TCEELs is plotted in Fig. 1(a). First, according to this mechanism, the rare earth ions populating the ground state get excited to a high-energy state. Then the ions relax to the two TCEELs to reach a transient thermoequilibrium before decaying to other energy levels if both the relaxation rate γ_{21} and the thermal excitation rate γ_{12} are much faster than the overall decay of the population in the two levels. In such a case, the population of these two TCEELs is governed by the Boltzmann distribution law, so that the FIR satisfies the equation

$$\mathrm{FIR} = A \exp\left(\frac{-\Delta E}{k_B T}\right), \quad (1)$$

where A is a constant, ΔE is the energy difference between the two TCEELs, k_B is the Boltzmann constant, and T is absolute temperature. With this formula, the FIR can be used to calibrate temperature. According to the detailed balancing principle,[21] the ratio of the two rates at temperature T is given by the equation

$$\frac{\gamma_{12}}{\gamma_{21}} = \frac{g_2}{g_1} \exp(-\Delta E/k_B T), \quad (2)$$

where g_2 and g_1 are the degeneracies of the two levels. While the relaxation rate γ_{21} resulting from a phonon-emission process usually decreases moderately with decreasing temperature, γ_{12} decreases dramatically with temperature. Hence, when the

Key Laboratory of Strongly Coupled Quantum Matter Physics, Chinese Academy of Sciences, School of Physical Sciences, University of Science and Technology of China, No. 96 Jinzhai Road, Hefei, Anhui Province, 230026, P. R. China. E-mail: yinmin@ustc.edu.cn; ckduan@ustc.edu.cn

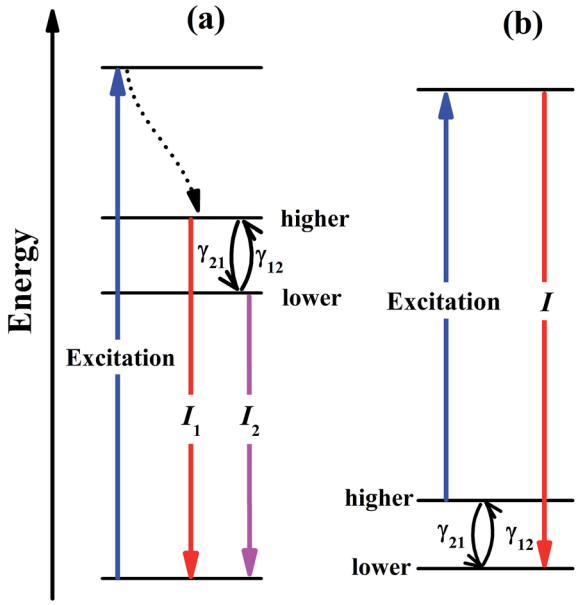

Fig. 1 The diagrams of energy levels and the transitions involved in the FIR method based on thermally coupled excited energy levels (a) and our method based on two thermally coupled ground energy levels used in this work (b).

temperature is sufficiently low, the rate of thermal excitation from the lower to the upper level is so slow that thermoequilibrium can no longer be achieved before the population decays to other lower energy levels. As a result, the thermal coupling condition is no longer valid at such low temperatures, which has been observed experimentally.[20]

The UC process is usually used in FIR-based techniques for various applications, and one of its advantages is that it is less disturbed than are other processes by stray scattered light, which is usually Stokes type, *i.e.*, red-shifted, and hence is not in the detection wavelength region. However, as the quantum efficiency of UC (defined as the ratio of the number of upconverted photons to that of the incident photons) is usually very low (up to about 1%) under weak to medium excitation strengths suitable for optical thermometry,[16,22] there is a trade-off between achieving high temperature accuracy and increasing the signal-to-noise ratio: reducing the heating effect of the laser requires decreasing the incident (usually infrared) laser power, while increasing the signal-to-noise ratio requires increasing the laser power. Some other schemes based on spectral shift,[23–25] absolute intensity[26–28] and luminescence decay lifetime[29–31] have also been explored. Also note that almost all of these techniques suffer from the drawback that only a small portion of the emitted light is in the wavelength range of detection.

In this work, we considered a different optical thermometry mechanism, one involving the temperature dependence of the thermal population of low-lying levels just above the ground level, as plotted in Fig. 1(b). The population of these low-lying levels follows the Boltzmann law, as long as the excitation is not strong enough to substantially disturb the population. The population of the higher level in Fig. 1(b) increases with temperature, so that after the excitation by a laser pulse, the population transferred to the luminescent level increases with temperature, the luminescence intensity of which can then be calibrated to the sensing temperature. In contrast to the mechanism in Fig. 1(a), the thermal coupling in Fig. 1(b) can be retained at low temperatures as long as the excitation is not too strong.

In our previous work,[32] we resonantly excited Eu^{3+} ions in Y_2O_3 from $^7F_2$ to $^5D_0$ and then detected the $^5D_0 \rightarrow {}^7F_4$ emission intensity to calibrate the temperature. However, the $^5D_0$ luminescence of Y_2O_3:Eu^{3+} was overwhelmingly dominated by the transition to the $^7F_2$ multiplet that overlapped with the excitation wavelength, so only a tiny portion of the $^5D_0$ emission, which amounted to about 1% of the total emission intensity, was used.

In order to avoid the above disadvantage, we developed in the current work a new temperature sensing scheme with Eu^{3+}-doped $Ca_3Sc_2Si_3O_{12}$ (CSSO:Eu^{3+}) as a model system. The Eu^{3+} ion dopant was found to substitute for the Ca^{2+} ion in a dodecahedral site with D_2 symmetry,[33,34] which could roughly be modeled as D_{4d} when only considering the nearest coordinating O^{2-} ions. As $^5D_0 \rightarrow {}^7F_2$ is strictly forbidden by D_{4d} point group selection rules, Eu^{3+} ions in this host actually produced an intense luminescence of $^5D_0 \rightarrow {}^7F_1$ and $^5D_0 \rightarrow {}^7F_4$ relative to that of $^5D_0 \rightarrow {}^7F_2$, much different than that of Eu^{3+} ions in Y_2O_3, where $^5D_0 \rightarrow {}^7F_2$ luminescence dominated the emission. Hence, determining the emission intensity of either the $^5D_0 \rightarrow {}^7F_1$ or $^5D_0 \rightarrow {}^7F_4$ transition or the total of the two is expected to realize temperature sensing with all of the advantages mentioned above.

2. Experimental procedure

Powder samples of the garnet CSSO doped with Eu^{3+} ions were prepared by carrying out a solid state reaction at a high temperature. High-purity $CaCO_3$, SiO_2, Sc_2O_3 and Eu_2O_3 in a stoichiometric ratio were thoroughly mixed and pressed into a pellet to form $Ca_{2.94}Eu_{0.04}Sc_2Si_3O_{12}$ samples. The samples were subjected to three heat treatments at 1450 °C for 3 h in an air atmosphere with intermediate grindings.[33]

The as-prepared phosphors were characterized by using an X-ray diffractometer (MAC Science Co., Ltd, MXP18AHF, Tokyo, Japan) with nickel-filtered Cu K_α radiation (λ = 0.15418 nm), and with the accelerating voltage and tube current being 40 kV and 100 mA, respectively. The photoluminescence excitation spectrum and the temperature dependence of the emission spectrum were investigated by using a double monochromator (Model Jobin-Yvon HRD-1) equipped with a Hamamatsu R928 photomultiplier. The excitation source was a tunable laser system (Model Opolette 355 LD OPO system) with a pulse duration of 7 ns. The decay curves were recorded using a Tektronix TDS2024 digital storage oscilloscope. For the measurements at low temperature, the powder sample was pressed into a round tablet with a thickness of 0.8 mm and diameter of 8.0 mm. And then the tablet was glued to a copper pedestal fixed in a closed-cycle cryostat with cryogenic glue. The temperature of the sample was controlled by the attached copper pedestal,

whose temperature was in turn controlled to be in the range 150–300 K by using a WC50 helium compressor and a Lake Shore Model 321 temperature controller.

3. Results and discussion

The crystal structure was identified according to the XRD pattern in Fig. 2. All of the diffraction peaks of the sample were found to match well with the standard CSSO (JCPDS no. 74-1578), and no obvious additional peaks of other phases were found, indicating that Eu^{3+} ions entered the host.

Fig. 3 shows the excitation spectrum monitoring the 611 nm-wavelength emission and the emission spectrum under 355 nm-wavelength excitation of CSSO:Eu^{3+} acquired at room temperature. Unlike Eu^{3+} ions in many other hosts where the $^5D_0 \rightarrow {}^7F_1$ and $^5D_0 \rightarrow {}^7F_4$ transitions have been shown to be much weaker than the $^5D_0 \rightarrow {}^7F_2$ transition, the Eu^{3+} ions in CSSO produced very strong $^5D_0 \rightarrow {}^7F_1$ and $^5D_0 \rightarrow {}^7F_4$ transitions, comparable to that of $^5D_0 \rightarrow {}^7F_2$, as a result of Eu^{3+} replacing Ca^{2+} in the site with an approximate D_{4d} local symmetry. The emission spectrum showed a $^5D_0 \rightarrow {}^7F_2$ transition peak at a wavelength of 610.6 nm.

The mechanism of the temperature-sensing scheme is depicted in Fig. 4(a). Initially, the Eu^{3+} ions populated at a $^7F_2$ Stark level (denoted as $^7F_{2,ini}$). According to the Boltzmann distribution law, the temperature-dependent population of the $^7F_{2,ini}$ Stark level is given by

$$N_{ini}(T) = N\frac{g_{ini}\exp\left(-\frac{\Delta E_{ini}}{k_B T}\right)}{\sum_i g_i \exp\left(-\frac{\Delta E_i}{k_B T}\right)}, \quad (3)$$

where $i = (1, 2 \ldots)$ represents the index of the Stark energy levels of ^7F_J, g_i is the degeneracy of level i, and ΔE_i is the energy difference between level i and the ground level, which is labeled as 1. Eqn (3) becomes similar to eqn (2) at low temperatures. The Eu^{3+} ions populated at $^7F_{2,ini}$ became resonantly excited to the $^5D_0$ level under incident light with a wavelength of 610.6 nm. Then the emissions from $^5D_0$ terminating at $^7F_1$ or $^7F_4$ were detected, with the results in the 580–602 nm and 690–830 nm ranges plotted in Fig. 4(b). For a temperature-dependent population of Eu^{3+} ions in the $^7F_{2,ini}$ level obeying the Boltzmann distribution at thermal equilibrium, the number of Eu^{3+} ions being excited to $^5D_0$ was expected to vary strongly with temperature, as for the emission intensity. This expectation was confirmed by the measured emission spectra for three representative temperatures plotted in Fig. 4(b). Such temperature-dependent luminescence intensities can be calibrated to measure the temperature surrounding Eu^{3+} ions. Apart from the featured sharp emissions from Eu^{3+} ions, we observed unexpectedly a broad band in the range of 690–830 nm, which was too weak to be detected under a 355 nm-wavelength excitation (Fig. 3). We attributed this broad band to the presence of trace amounts of Eu^{2+} in the sample,[35] whose emission intensity under a 610.6 nm-wavelength excitation stood out relative to that of Eu^{3+}, as a result of a parity-allowed strong electric dipole transition between the $4f^7$ ground configuration and the parity-flipped $(4f)^6 5d$ excited configuration.[36]

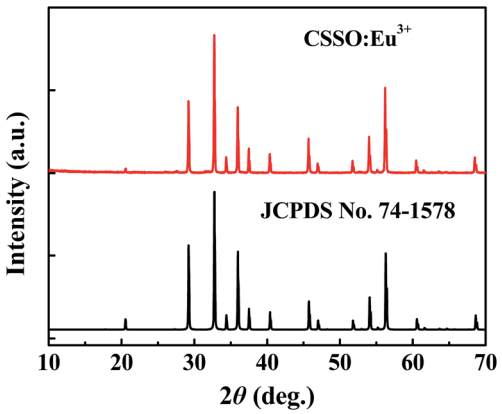

Fig. 2 XRD pattern of CSSO:Eu^{3+} powder sample.

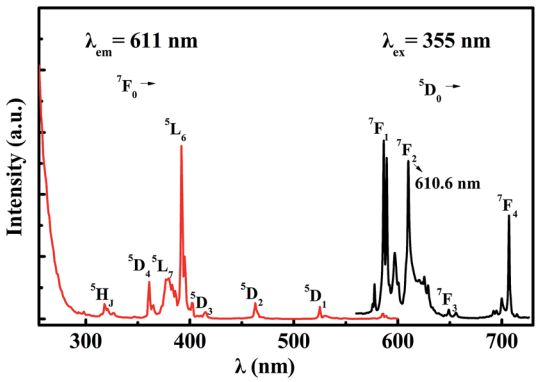

Fig. 3 Excitation spectrum (red curve) and emission spectrum (black curve) of Eu^{3+} in CSSO at room temperature.

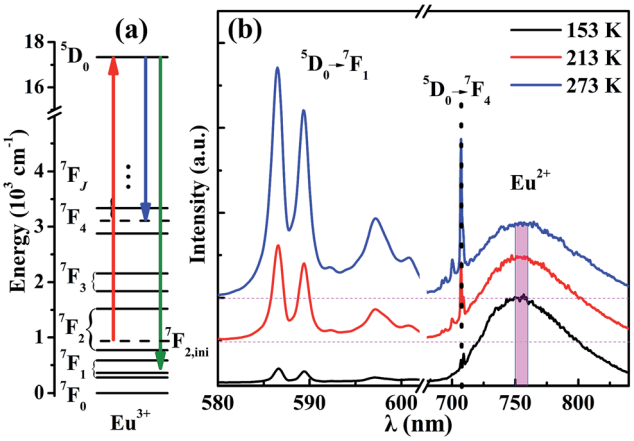

Fig. 4 (a) Simplified energy level diagram showing transitions excited from $^7F_2$ to $^5D_0$ and emission transitions originating from $^5D_0$ to $^7F_1$ and $^7F_4$. (b) Luminescence intensities corresponding to the $^5D_0 \rightarrow {}^7F_1$ and $^5D_0 \rightarrow {}^7F_4$ transitions of Eu^{3+} and Eu^{2+} at various temperatures.

In order to depict this temperature-dependent variation quantitatively, the integrated intensities from 580 nm to 602 nm at various temperatures were calculated, as shown in Fig. 5(a). The filled black rectangles are the experimental data, which well fit the Arrhenius formula $I = A\exp(-B/T)$ with $B = 1008$ K, as shown by the red solid curve in Fig. 5(a). From this curve, we obtained the relative sensitivity $S_R = I^{-1}\mathrm{d}I/\mathrm{d}T = BT^{-2}$, which is plotted in Fig. 5(b). It should noted that the constant B was determined to have a value of 1008 K, corresponding to an effective energy difference ΔE_{eff} of 700 cm^{-1}, much smaller than the 910 cm^{-1} ΔE_{real} energy difference between $^7F_2$ and $^7F_0$ obtained from the emission spectrum. The error δ is defined as[2] $\delta = |\Delta E_{\mathrm{real}} - \Delta E_{\mathrm{eff}}|/\Delta E_{\mathrm{real}}$, which was calculated to be 23% in the case of CSSO:Eu^{3+}. The error δ is a key parameter which reflects how much the effective energy difference ΔE_{eff} deviates from the real energy difference ΔE_{real}. The value of δ we found resulted from the variation of the population of $^7F_2$, because the positions of the energy levels of Eu^{3+} changed with temperature. Some other factors such as absorption efficiency and luminescence quantum efficiency may have also changed with temperature, but are beyond the scope of our discussion.

Measuring the broadband luminescence in the near-infrared region may serve as another way to calibrate temperature. Fig. 6(a) shows the FIR of the integrated fluorescence intensity of $^5D_0 \rightarrow {}^7F_1$ of Eu^{3+} with respect to that of Eu^{2+}. The integration interval of the former was carried out from 580 nm to 602 nm, and of Eu^{2+} from 750 nm to 760 nm (see Fig. 4(b)). The inset of Fig. 6(a) shows the dependence of the corresponding relative sensitivity on temperature.

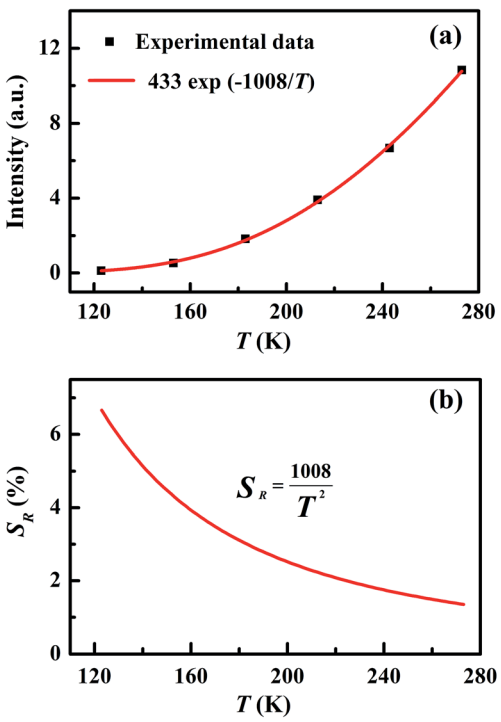

Fig. 5 Temperature-dependent absolute intensity (a) and relative sensitivity (b) of $^7F_1$.

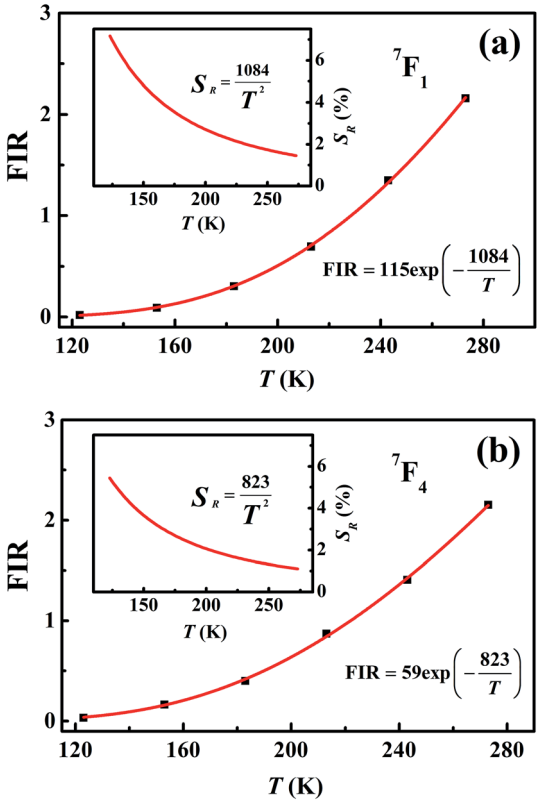

Fig. 6 (a) Temperature-dependent FIR and relative sensitivity of $^7F_1$. (b) Temperature-dependent FIR and relative sensitivity of $^7F_4$.

The same treatment for $^7F_4$ as that for $^7F_1$ is shown in the plot in Fig. 6(b), except that Fig. 6(a) shows the ratio of integrated fluorescence intensities while Fig. 6(b) shows the ratio of peak heights instead. The luminescence of $^7F_4$ and Eu^{2+} overlap around 707 nm and the peak height for $^7F_4$ was determined by the whole peak height of $^7F_4$ and Eu^{2+} at 707 nm subtracting the peak height for Eu^{2+} at 707 nm whose value is easy to evaluate from the shape of the broadband. The peak height for Eu^{2+} was given by the average value of the intensity for Eu^{2+} between wavelengths of 750 nm and 760 nm (Fig. 4(b)). The advantage of using the fluorescence intensity ratio over the absolute fluorescence intensity lies in that the former corrects for fluctuations of the excitation light, and for changes in the environment and the measurement conditions.

4. Conclusions

In conclusion, an optical thermometry mechanism using the thermal population of Eu^{3+} ions in low-lying levels was demonstrated with CSSO:Eu^{3+}. Under excitation with 610.6 nm-wavelength light, the CSSO:Eu^{3+} material showed excellent fluorescence properties and temperature-dependent luminescence properties for temperature sensing with a relative sensitivity of $1008/T^2$. The wavelength of the emitted light was shorter than that of the excitation light, and such a blue shift was able to reduce errors caused by stray light. The thermal equilibrium between the ground state $^7F_0$ and $^7F_2$ was naturally guaranteed

even at low temperatures, so CSSO:Eu^{3+} was suitable for temperature sensing below room temperature. Furthermore, a broadband emission was observed at a wavelength of about 750 nm, which was attributed to the luminescence of Eu^{2+} trace impurities, and can be chosen as a reference. Calculating the FIR between $^5D_0 \rightarrow {}^7F_1$ of Eu^{3+} and Eu^{2+} can serve as another way of sensing temperature, and benefits from the advantages of FIR techniques. The experimental data can be fitted using the formula $I = A\exp(-B/T)$ for the emissions to both $^7F_1$ and $^7F_4$ multiplets, and a relative sensitivity S_R of $1008/T^2$ was obtained for the $^7F_1$ case, with a value of 1.35% at 273 K.

Acknowledgements

This work was financially supported by the National Key Research and Development Program of China (Grant No. 2016YFB0701001); National Key Basic Research Program of China (Grant No. 2013CB921800) and the National Natural Science Foundation of China (Grant No. 11604037, 11374291, 11574298 and 11404321).

References

1 D. Jaque and F. Vetrone, *Nanoscale*, 2012, **4**, 4301–4326.
2 X. Wang, Q. Liu, Y. Bu, C. Liu, T. Liu and X. Yan, *RSC Adv.*, 2015, **5**, 86219–86236.
3 C. D. S. Brites, P. P. Lima, N. J. O. Silva, A. Millán, V. S. Amaral, F. Palacio and L. D. Carlos, *Nanoscale*, 2012, **4**, 4799–4829.
4 X. Wang, R. J. Meier, M. Schäferling, S. Bange, J. M. Lupton, M. Sperber, J. Wegener, V. Ondrus, U. Beifuss, U. Henne, C. Klein and O. S. Wolfbeis, *Adv. Opt. Mater.*, 2016, **4**, 1854–1859.
5 W. Tang, S. Wang, Z. Li, Y. Sun, L. Zheng, R. Zhang, B. Yang, W. Cao and M. Yu, *Appl. Phys. Lett.*, 2016, **108**, 061902.
6 W. Xu, Q. Song, L. Zheng, Z. Zhang and W. Cao, *Opt. Lett.*, 2014, **39**, 4635–4638.
7 X. Tian, X. Wei, Y. Chen, C. Duan and M. Yin, *Opt. Express*, 2014, **22**, 30333–30345.
8 K. Zheng, Z. Liu, C. Lv and W. Qin, *J. Mater. Chem. C*, 2013, **1**, 5502–5507.
9 Z. Boruc, M. Kaczkan, B. Fetlinski, S. Turczynski and M. Malinowski, *Opt. Lett.*, 2012, **37**, 5214–5216.
10 Y. Y. Bu, S. J. Cheng, X. F. Wang and X. H. Yan, *Appl. Phys. A*, 2015, **121**, 1171–1178.
11 P. Du, L. Luo and J. S. Yu, *J. Alloy. Compd.*, 2015, **632**, 73–77.
12 S. Zhou, S. Jiang, X. Wei, Y. Chen, C. Duan and M. Yin, *J. Alloys Compd.*, 2014, **588**, 654–657.
13 V. Kumar, S. Som, S. Dutta, S. Das and H. C. Swart, *RSC Adv.*, 2016, **6**, 84914–84925.
14 P. Du, L. Luo, W. Li and Q. Yue, *J. Appl. Phys.*, 2014, **116**, 014102.
15 D. He, C. Guo, S. Jiang, N. Zhang, C. Duan, M. Yin and T. Li, *RSC Adv.*, 2015, **5**, 1385–1390.
16 S. Zhou, K. Deng, X. Wei, G. Jiang, C. Duan, Y. Chen and M. Yin, *Opt. Commun.*, 2013, **291**, 138–142.
17 S. Senapati and K. K. Nanda, *Phys. Chem. Chem. Phys.*, 2016, DOI: 10.1039/C6CP06608A.
18 X. Wang, Q. Liu, P. Cai, J. Wang, L. Qin, T. Vu and H. J. Seo, *Opt. Express*, 2016, **24**, 17792–17804.
19 L. Xing, Y. Xu, R. Wang, W. Xu and Z. Zhang, *Opt. Lett.*, 2014, **39**, 454–457.
20 S. A. Wade, S. F. Collins and G. W. Baxter, *J. Appl. Phys.*, 2003, **94**, 4743–4756.
21 J. Berger, *J. Stat. Mech.: Theory Exp.*, 2010, **07**, P07022–P0703321.
22 J. Zhou, Z. Liu and F. Li, *Chem. Soc. Rev.*, 2012, **41**, 1323–1349.
23 A. Narayanaswamy, L. F. Feiner, A. Meijerink and P. J. van der Zaag, *ACS Nano*, 2009, **3**, 2539–2546.
24 L. M. Maestro, E. M. Rodríguez, F. S. Rodríguez, M. C. Iglesias-de la Cruz, A. Juarranz, R. Naccache, F. Vetrone, D. Jaque, J. A. Capobianco and J. G. Solé, *Nano Lett.*, 2010, **10**, 5109–5115.
25 Q. Dai, Y. Zhang, Y. Wang, M. Z. Hu, B. Zou, Y. Wang and W. W. Yu, *Langmuir*, 2010, **26**, 11435–11440.
26 E. H. Song, S. Ding, M. Wu, S. Ye, F. Xiao, G. P. Dong and Q. Y. Zhang, *J. Mater. Chem. C*, 2013, **1**, 4209–4215.
27 C. Gota, K. Okabe, T. Funatsu, Y. Harada and S. Uchiyama, *J. Am. Chem. Soc.*, 2009, **131**, 2766–2767.
28 S. Uchiyama, N. Kawai, A. Prasanna de Silva and K. Iwai, *J. Am. Chem. Soc.*, 2004, **126**, 3032–3033.
29 N. Rakov, S. A. Vieira, Q. P. S. Silva and G. S. Maciel, *Sens. Actuators, B*, 2015, **209**, 407–412.
30 D. Chen, Z. Wan and Y. Zhou, *Sens. Actuators, B*, 2016, **226**, 14–23.
31 O. A. Savchuk, P. Haro-González, J. J. Carvajal, D. Jaque, J. Massons, M. Aguiló and F. Díaz, *Nanoscale*, 2014, **6**, 9727–9733.
32 S. Zhou, X. Li, X. Wei, C. Duan and M. Yin, *Sens. Actuators, B*, 2016, **231**, 641–645.
33 M. Bettinelli, A. Speghini, F. Piccinelli, A. N. C. Neto and O. L. Malta, *J. Lumin.*, 2011, **131**, 1026–1028.
34 K. Binnemans, *Coord. Chem. Rev.*, 2015, **295**, 1–45.
35 I. V. Berezovskaya, V. P. Dotsenko, A. S. Voloshinovskii and S. S. Smola, *Chem. Phys. Lett.*, 2013, **585**, 11–14.
36 P. A. Tanner and C. Duan, *Coord. Chem. Rev.*, 2010, **254**, 3026–3029.

